

# New Image Analysis Method for Determination of the Inter-Fibre Pore Size Intensity of Polyester Woven Barrier Fabrics

DOI: 10.5604/01.3001.0012.1315

Dresden University of Technology,  
Faculty of Mechanical Science and Engineering,  
Institute of Textile Machinery  
and High Performance Material Technology,  
Hohe Straße 6, Dresden, Germany  
\*E-mail: recep\_tuerkay.kocaman1@tu-dresden.de

## Abstract

Porosity is an important characteristic of a filter textile, which affects permeability and retention properties. Determination of the inter-yarn and inter-fibre pore sizes of barrier textiles is also required to assess the filter behaviour of these textiles. In this study, a software tool was developed to detect the inter-fibre pore size distribution and pore size intensity of multifilament woven barrier fabrics using cross-section images. Fabrics were chosen according to their fabric construction parameters, such as the fabric index, weft yarn filament fineness and weft yarn structure (flat or textured). Microscopic cross-section images of weft yarns were taken, processed to binary images, and analysed with respect to the pore size distribution, number of pore lengths and pore intensity. It was also analysed how the fabric index, filament cross-section and filament fineness affect the inter-fibre pore lengths and separation level proposed. It was found that weft yarns with wider lengths and lower height showed wider inter-fibre pores. Inter-fibre pores decreased with a decrease in filament fineness. Moreover the separation level proposed deviated from the 90% level depending on the fabric index. This deviation was very small in samples with reduced filament fineness and textured samples. The separation level proposed will be useful to understand the effect of fabric construction parameters to obtain targeted properties regarding inter-fibre and inter-yarn pore size.

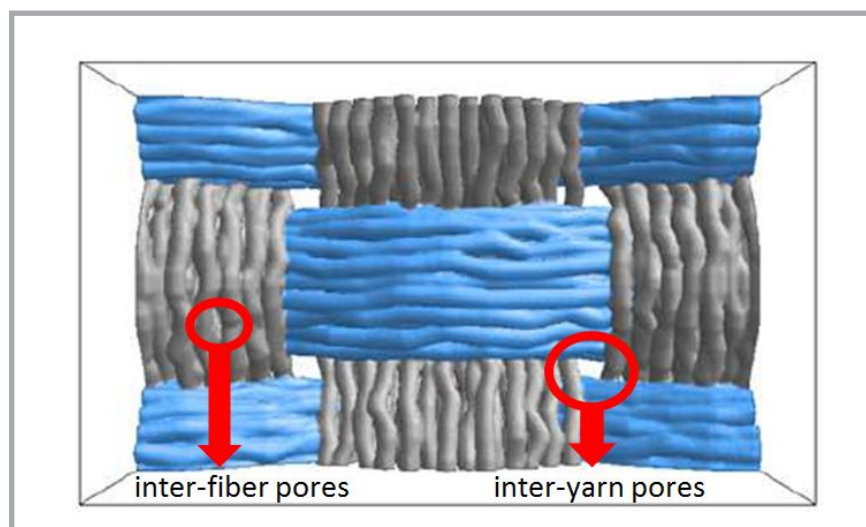
**Key words:** inter-fibre pore size, porosity, image processing, barrier textiles.

## Introduction

High density polyester (PES) multifilament weaves are widely used for the manufacturing of protective textiles, e.g. surgical gowns for the operating room [1]. The pore structure of a multifilament woven fabric has already been classified as the combination of inter-fibre and inter-yarn pores, whereas inter-fibre pores refer to those between filaments of a yarn and inter-yarn pores to those between yarns in the warp and weft direction of the woven fabric [2, 3] (*Figure 1*). This combination is an essential factor involved in the assessment of filter properties [4], preventing the strike-through of contaminated fluids and particles through the fabric as well as defining air and vapour permeability [5, 6]. These pore sizes are affected by fabric construction parameters (fabric index, weft yarn density, weft yarn count and yarn structure) [7], and al-

terations to these parameters also lead to morphological changes, such as porosity as well as air and water vapour permeability [7, 8]. The inter-fibre porosity of woven textiles acts as a key factor due to its considerable effect on the filtration properties of textiles, which constitute the main mechanism for fine filtration. In order to ensure the necessary filtration against bacteria and germs, the inter-fibre porosity of hospital gowns should be taken into account. *Staphylococcus aureus* is a pathogenic bacterium, with particle sizes from 0.8  $\mu\text{m}$  to 1.2  $\mu\text{m}$ , that can cause infections, particularly during

surgery [9, 10]. Analysis of the inter-fibre porosity of woven barrier textiles might be a helpful tool to determine if these textiles possess the required barrier property against nosocomial infections. These are hospital-acquired infections caused by bacteria like *Staphylococcus aureus* and are major causes of death and serious illness. Furthermore this analysis can provide information for the simulation of the filter properties of multifilament woven textiles [8, 11]. For these reasons, it is of great importance to determine the porosity deformation of polyester multifilament woven fabrics.



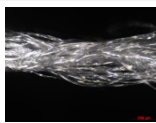


**Figure 1.** Representation of inter-fibre pores (left) and inter-yarn pores (right) in a multifilament woven fabric [11].

**Table 1.** Design of experiment – fabric specifications with construction and process parameters.

Sample number	Warp yarn	Weft yarn	Warp density, cm <sup>-1</sup>	Weft density, cm <sup>-1</sup>	Binding	Fabric index (Walz-Luibrand)	Machine speed, rpm
1	Yarn 1	Yarn 1	68	22	Plain 1/1	0.55	300
2	Yarn 1	Yarn 1	68	27	Plain 1/1	0.68	300
3	Yarn 1	Yarn 2	68	27	Plain 1/1	0.68	300
4	Yarn 1	Yarn 3	68	27	Plain 1/1	0.68	300

**Table 2.** Yarn specifications.

Yarn type	Warp yarn	Longitudinal view	Yarn fineness, dtex	Filament fineness, dtex	Yarn diameter, mm	Usage in weave – effect
Yarn 1	Multifilament 100 dtex f40 flat – round		100	2.5	9.57x10 <sup>-2</sup>	Warp and weft yarn
Yarn 2	Multifilament 100 dtex f128 flat – round		100	0.78	9.57x10 <sup>-2</sup>	Weft yarn – effect of filament fineness
Yarn 3	Multifilament 100 dtex f128 textured – angular		100	0.78	9.57x10 <sup>-2</sup>	Weft yarn – effect of filament cross section

There are several methods used to determine the pore sizes of textiles, e.g. the mercury intrusion porosimetry method [12, 13, 16], the bubble point [14-16] as part of the capillary flow porosimetry method, the liquid displacement method [17-20], and image analysis techniques [21-28]. The image analysis technique has been widely used for the determination of pore sizes in a 2D-plane image of woven fabrics and membranes. In study [22], image analysis technology was used to determine the effective pore size, pore diameter and the total number of pores of nonwoven and woven fabrics. With the same approach, a geometric parameter termed the effective pore diameter was defined to characterise the particle permeation performance in porous filtration membranes [23]. Scanning electron microscopy (SEM) and transmission electron microscopy (TEM) images were analysed to determine the surface morphology of fabrics and to calculate pore diameters [23, 24]. The ratio between the area of the pores and the total area of the image region investigated was defined as the ‘porous area fraction’, and this area was referred to as the porosity of the material in a 2D plane image [25]. Binarised images were also processed to determine the in situ porosity change of carbon felt electrodes under various percentage compressions [26]. Pixel counts of dark and bright regions were recorded to calculate the porosity changes. In another study, high-resolution images of

textile implants were processed for the calculation of porosity [27]. A resolution of 10 µm was achieved with the camera lens chosen. Coloured pictures were taken, which were subsequently converted into grey scale images using transform coefficients and then transferred into binary images via adaptive thresholding. The same method was applied to detect 2D porosity changes during uniaxial loading of textile implants with a mesh structure [28]. However, the focus of these scientific studies was almost exclusively on the surface porosity in order to analyse the inter-yarn porosity of textile materials.

The inter-fibre porosity of woven fabrics was also determined with image analysis methods using ImageCC© software [21]. The microscopic images processed were represented as a two-phase texture (filament and pores). Pore lengths were measured with linear analysis methods using cutting lines in the horizontal and vertical directions. The distance between cutting lines could only be adjusted up to 2 µm, hence there is a lack of information for the area between two cutting lines due to this restriction. However, for precise determination of pore size distributions, this interspace should be taken into consideration. The quality of the analysis is dependent on that of the images; hence based on an image with high pixel resolution, even very fine distances can be measured, which might be essen-

tial for the interpretation of inter-fibre pores, particularly if bacteria with sizes between 0.8 µm and 2 µm are considered.

Although previous studies mentioned inter-fibre pore size distribution, they did not reveal how these pores are distributed along the yarn cross-section. Thus for the study described in this paper, a new image analysis method was developed in order to detect every single pixel in cross-section images of polyester multifilament woven barrier fabrics.

## Experimental

### Materials

Four types of woven fabrics were investigated in this study, whose construction parameters were varied. **Table 1** shows the fabric specifications, including construction and process parameters, which were chosen for the manufacturing of filter and barrier textiles. **Table 2** shows the specifications of the yarns chosen to manufacture the samples. These yarns were purchased from Trevira GmbH, Germany. The samples were woven on a rapier weaving machine – PTS4/E EasyLeno (Lindauer Dornier, Germany). A full-width temple guide was used because conventional temple guides were non-functional for our research purposes. Desizing of the samples was carried out in an air flow washing machine (Then, Hong Kong) using Felosan Fox (CHT)

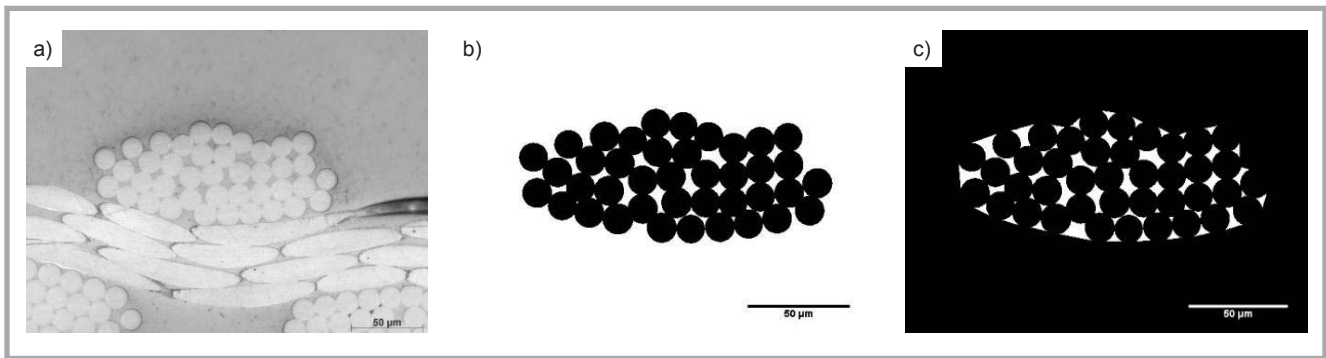


**Figure 2.** Image processing warp yarn cross section of sample 2: a) cross-section image, b) image processing, c) binarised image.

and Heptol B 81 200% (CHT), and the pH of the liquor was adjusted to 8.8 with sodium carbonate. Samples were treated with liquor (liquor ratio: 1:2.5) at 90 °C for 40 minutes and then rinsed with cold water for 10 minutes. After desizing, the fabrics were fixed on a coating machine (Coatema Coating Machinery, Germany) at a temperature of 200 °C.

Samples with different weft densities were manufactured to evaluate the effect of the fabric index on inter-fibre porosity. The filament fineness and texture of weft yarns were varied for the same reason. Fabric indices were calculated theoretically according to Walz-Luibrand [29], in which the fabric count, yarn diameter and yarn density were merged together. It was calculated using **Equation (1)**:

$$WI = \frac{b \cdot (d_{wp} + d_{wf})^2 \cdot (n_{wp} \cdot n_{wf})}{100} \quad (1)$$

where  $b$  is the weave coefficient (For Plain 1/1 = 1, Twill 2/2 = 0.56, Twill 3/2 = 0.49 and Satin 4/1 = 0.5),  $d$  the yarn diameter in mm, and  $n$ , the number of yarns per cm. Subscripts  $wp$  and  $wf$  indicate warp and weft yarns, respectively. The yarn diameters in **Table 2** were calculated using **Equation (2)**:

$$d(\text{mm}) = \left( \sqrt{\frac{T_y \cdot 4}{\pi \cdot \rho_y \cdot 10^5}} \right) \cdot 10 \quad (2)$$

where  $d$  is the diameter of yarn in mm,  $T_y$  the yarn count in tex, and  $\rho_y$  is the yarn material density in g/cm<sup>3</sup> (PES = 1.39 g/cm<sup>3</sup>).

## Methods

### Preparation of cross-sections

The woven structure was cut to dimensions of 1.5 cm x 0.5 cm and subsequently embedded into epoxy resin in a sample carrier. After 8 hours of hardening time, it was smoothed and polished with a grinding device (Struers, Germany). Cross-section images were taken with a light microscope – Axio Imager M1m

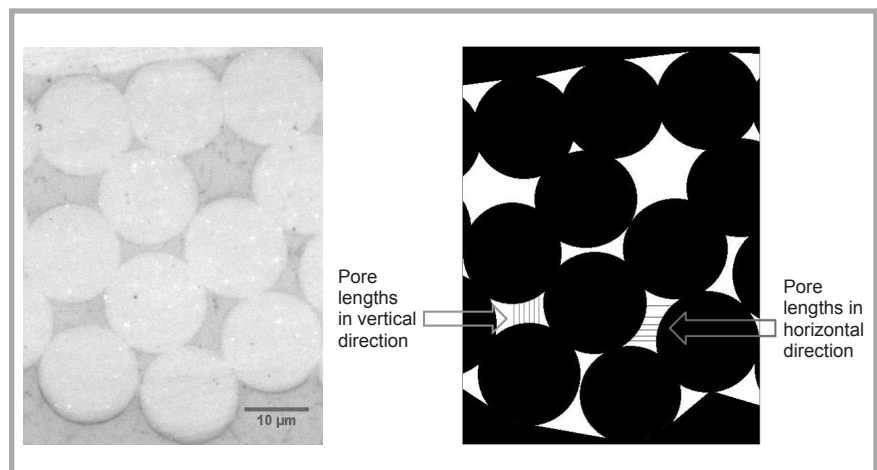


**Figure 3.** Pore length measurement – binary image shows pore lengths measured in the horizontal direction with red lines and in the vertical direction with blue lines: a) original image, b) binary image

(Zeiss, Germany) at a magnification of 500, because the largest complete cross-section of each yarn sample could be achieved at this magnification.

### Analysis of cross-sectional image

Cross-section images were processed with a picture design program (Paint, Microsoft). The contours of the filaments in the cross-sectional view were defined. Subsequently in order to visualise only the inter-fibre pores of the cross section, the areas inside the contours and outside the yarn geometry were filled with black colour. The visualised images were binarised using ImageJ©. **Figure 2** illustrates an example of the image processing of the warp yarn cross-section of sample 2.

The images obtained had a resolution of 2584x1936 pixels and ratio of 9.3 pixels/1.0 µm, i.e. one pixel had a length of app. 0.107 µm. This enables the analysis of pore lengths down to 0.107 µm. For a precise analysis, one yarn cross-section was selected and arranged as displayed in **Figure 2**. The determination of pore lengths in the horizontal and vertical di-

rections followed the same approach as used for study [21]. The method presented enabled the processing of every pixel of the image in the horizontal or vertical direction. A software tool developed in Matlab© checked the image pixels in the horizontal and vertical directions and collected data of the connected white pixels. This analysis was performed for each row and column of the image, and the data collected were processed as a vector. Pixel  $P_{i,j+1}$  was also white when  $P_{i,j}$  was white for the horizontal direction. The algorithm collected the number of white pixels until  $P_{i,j+1}$  turned black and recorded every united white pixel as a pixel length and every length as a pore length. **Figure 3** illustrates pore length measurement in the horizontal and vertical directions. The pore number is the segmented pore length number of pores in the cross-section. The algorithm created another vector for the intensity of defined lengths. Pixel lengths were changed into “µm” lengths by using the calibration ratio. The number of inter-fibre pore lengths collected was used to create pore length intensity diagrams.



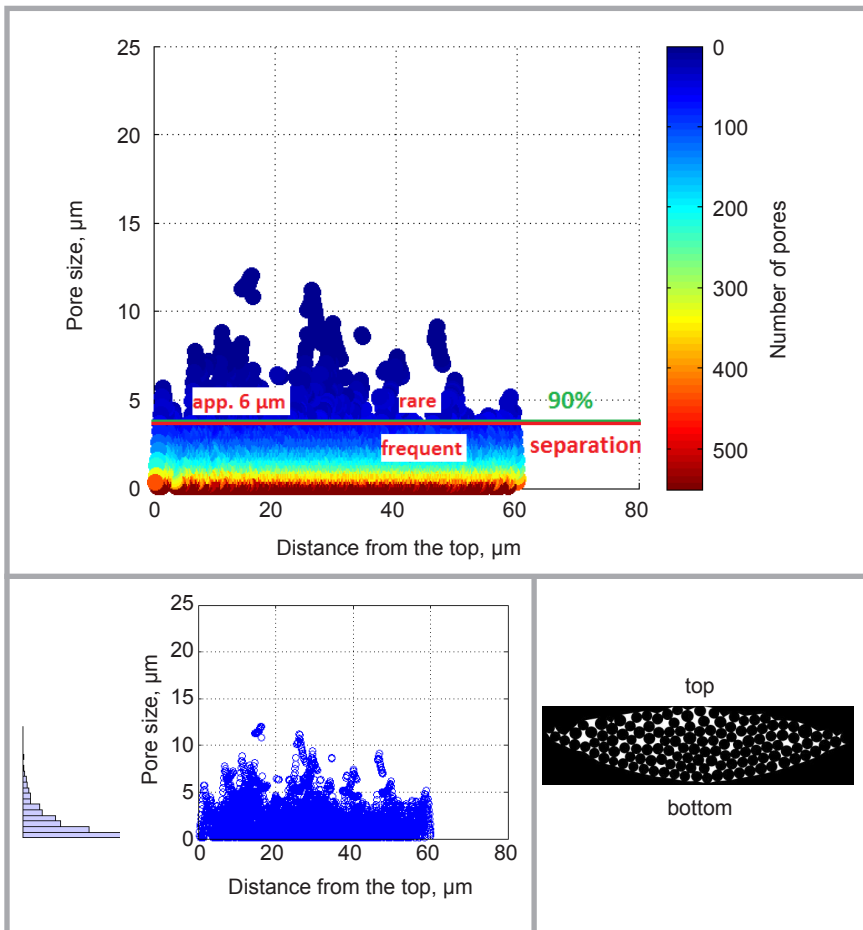


**Figure 4.** Pore length intensity diagram of sample 3 with frequency analysis (top), pore length scatter analysis (bottom-left) and its cross section (bottom-right).

Five cross sections from each sample were analysed and mean values used for the interpretation of results. A separation level was defined based on the pore length intensity diagram, revealing that the distribution of the pore length changed from a frequently distributed level to a rarely distributed level along the yarn cross-section. A 90% level was selected as a reference level to be compared with the separation level because a 90% value is considered as a confidence level in statistical distributions. In this case, it shows enormous pore lengths, which cannot be considered as inter-fibre pores in a particular pore size distribution.

## Results and discussion

The pore lengths and numbers that were determined based on the images arranged were used to plot pore length distribution and intensity diagrams. Weft yarn cross-section images were considered in order to analyse the influence of fabric and yarn construction. Cross-sections were analysed in the horizontal direction.

The algorithm developed is able to count inter-fibre pore lengths and plot intensity diagrams for cross-section images. **Figure 4** provides an explanation of the interpretation of the pore length intensity diagram of sample 3, as an example, using a colour bar, pore scatter diagram and its cross section. The scatter diagram shows the point cloud of pore lengths along the vertical direction. Blue arrows illustrate how the data were processed along the yarn cross-section from top to bottom. The colour bar shows the number of pores calculated by the algorithm, which was specially adjusted to every individual cross-section in order to reveal the change in the pore intensity of each cross-section.

The purpose of the scatter diagram was to obtain information regarding the detailed distribution of pore lengths along the vertical direction. Moreover it enabled determination of the level at which the distribution of pore lengths changes from frequently distributed to rarely distributed. The separation between frequently distributed pore lengths and

rarely distributed ones is marked with a dark red line; this level was defined as the “separation” level. The “90 %” level is also shown with a green line. For the given figure (**Figure 4**), it was observed that after approx. 4 μm the pore lengths began to distribute rarely along the vertical direction of the yarn cross section. Hence inter-fibre pore lengths of up to 4 μm occurred frequently at every vertical level of the yarn cross-section of sample 3. Moreover interpretations using the colour bar suggested that between 0.1 μm – 0.5 μm the number of pores increased to over 500 and decreased to around 60-70 at a level of 4 μm.

### Influence of fabric index on inter-fibre porosity

**Figure 5** illustrates the pore length distribution as a bar diagram, the pore length intensity as a scatter diagram, and weft yarn cross-sections of samples according to the influence of the fabric index.

An increase in the fabric index from 0.55 to 0.68 in plain woven samples led to smaller inter-fibre pore lengths, and the mean pore length decreased from 3.44 μm to 2.91 μm (**Figure 6-a**). Sample 1, with a fabric index of 0.55, revealed that 90% of pores were smaller than approx. 7.5 μm (**Figure 5.a**, pore size distribution diagram; green line marks the 90% level). In contrast to this value, sample 2, with a fabric index of 0.68, showed approx. 6 μm for the 90% level (**Figure 5.b**). This difference could be caused by the change in the cross-sectional geometry of weft yarns in the woven structure. Due to the increase in the fabric index, the weft yarns were more tightly packed, which also affected the inter-fibre porosity of the weft yarns. Woven fabrics with higher fabric indices (from a fabric index of 0.55 to one of 0.68) possessed more compressed weft yarn geometries in the horizontal direction. However, this resulted in wider weft yarn geometries in the vertical direction due to the increase in weft yarn density and corresponding change in yarn crimp. These wider weft lengths affected inter-fibre porosity in the horizontal direction. It was also observed that the newly defined separation level deviated from the 90% level depending on the fabric index. With a higher fabric index (fabric index: 0.68), sample 2 exhibited lower deviation from the 90% level compared to sample 1 (**Figure 6.b**).

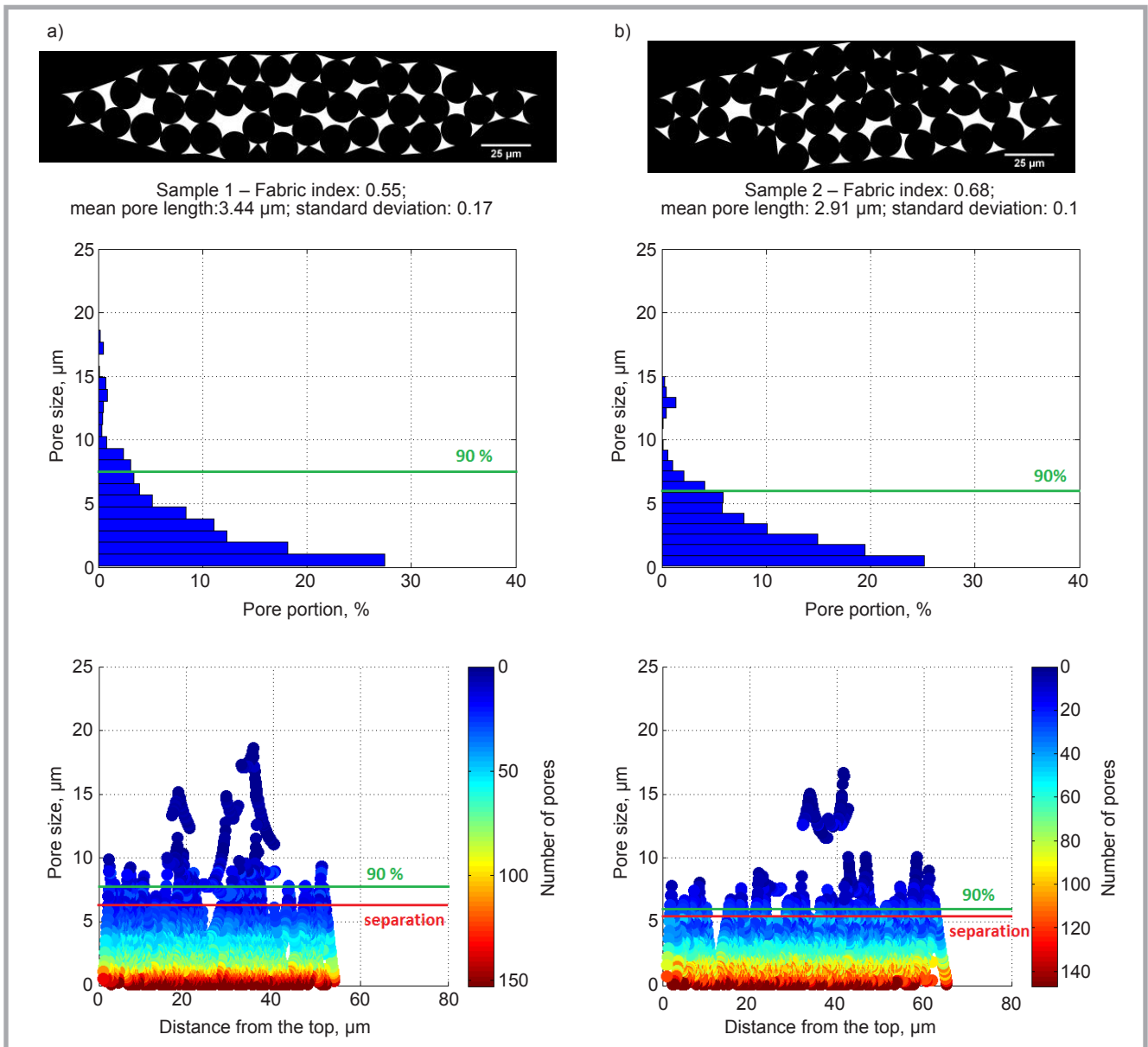


**Figure 5.** Cross-sectional image of the weft yarn, pore size distribution and pore intensity of woven fabrics in dependence on the varying fabric index

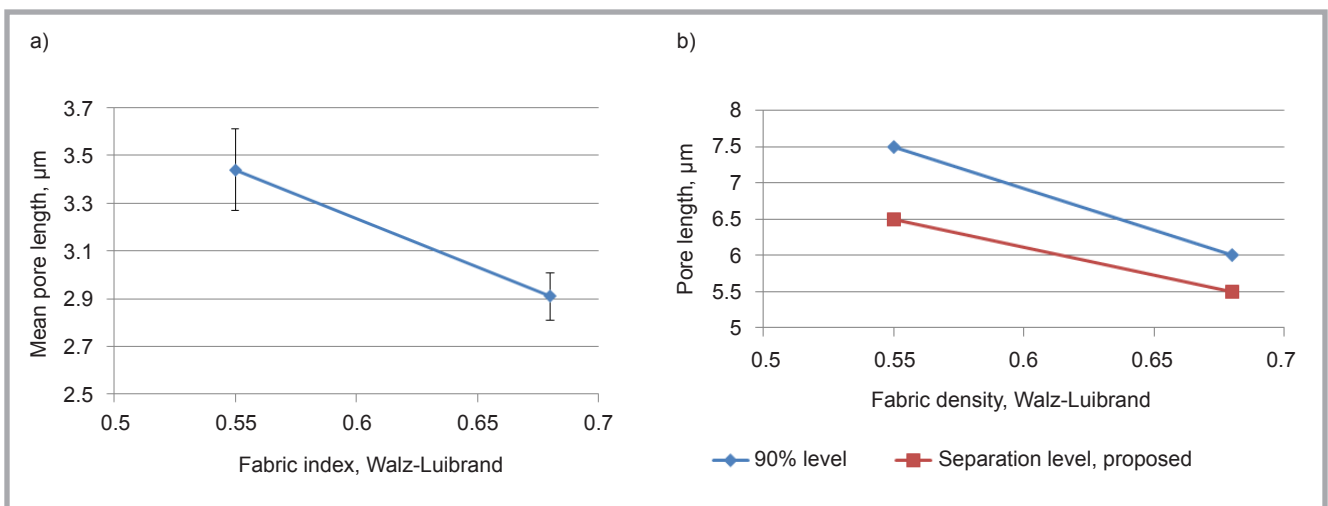


**Figure 6.** Influence of fabric index on mean pore length as well as 90% and separation level: a) Influence of fabric index on mean pore length b) Influence of fabric index on 90% and separation level.

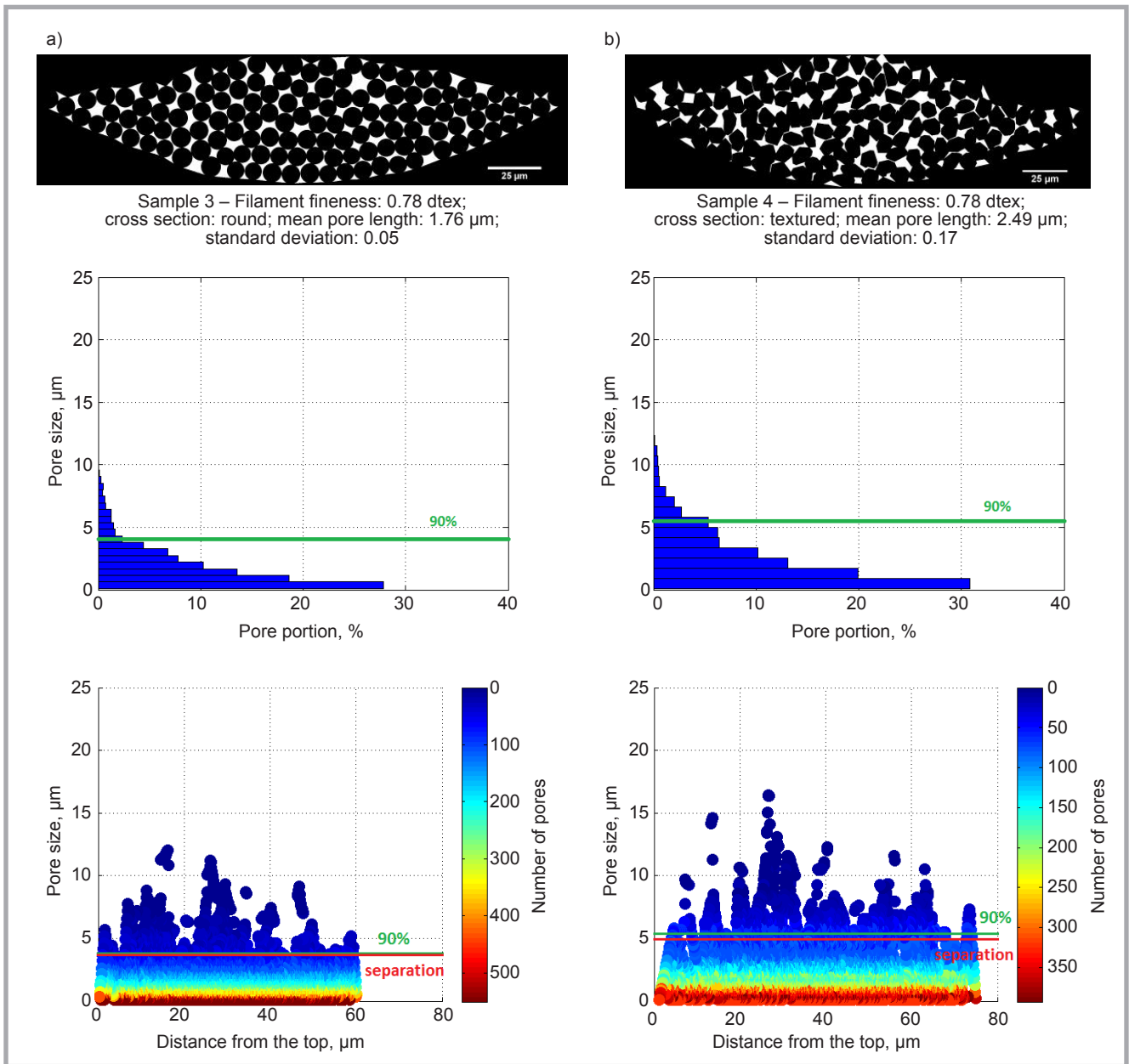


**Figure 7.** Cross-sectional image of weft yarn, pore size distribution and pore intensity of woven fabrics in dependence on varying filament cross section.

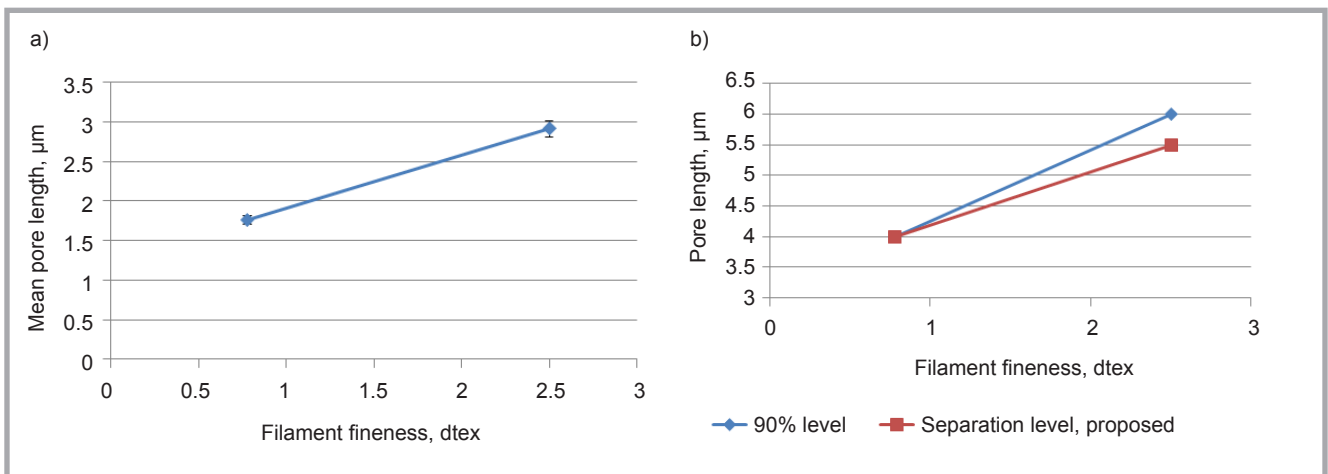


**Figure 8.** Influence of filament fineness on mean pore length as well as 90% and separation levels: a) Influence of filament fineness on mean pore length, b) Influence of filament fineness on 90% and separation levels

### Influence of filament cross-section on inter-fibre porosity

Textured weft yarn filament cross-sections exhibited greater inter-fibre mean pore lengths (Sample 4, *Figure 7.b*) compared to weft yarn filament cross-sections with flat filaments (Sample 3, *Figure 7.b*). The mean pore length of sample 4 was 2.49  $\mu\text{m}$ , whereas this value was 1.76  $\mu\text{m}$  in the case of sample 3, with the same filament fineness but with flat filaments. The 90% level of sample 4 was 5.5  $\mu\text{m}$ , whereas it was 4  $\mu\text{m}$  in sample 3. The texture process led to changes in the geometry of the filament cross-section (*Figure 7*), resulting in increased spaces between filaments, which, in turn, affects inter-fibre porosity. Sample 4 showed a separation level of around 5  $\mu\text{m}$  and 90% level of 5.5  $\mu\text{m}$  (*Figure 7.b*), whereas sample 3 showed a separation level of 4  $\mu\text{m}$  and 90% level of 4  $\mu\text{m}$ . Inferring that the cross section of textured yarns caused higher inter-fibre pore sizes, it thus affected the deviation of both levels considered as well.

### Influence of filament fineness on inter-fibre porosity

Lower filament fineness resulted in smaller inter-fibre pores (*Figure 8.a*). In the case of sample 2 (*Figure 5.b*), 90% of inter-fibre pores were smaller than approx. 6  $\mu\text{m}$ , whereas in sample 3 (*Figure 7.a*), 90% of inter-fibre pores were smaller than approx. 4  $\mu\text{m}$ . The mean pore length also decreased from 2.91  $\mu\text{m}$  to 1.76  $\mu\text{m}$ . Sample 3 had a separation level of around 4  $\mu\text{m}$ , which is smaller than that of sample 2, which is 5.5  $\mu\text{m}$ . From the color bars, it was observed that the number of pores in sample 3 was also higher than that in sample 2 (*Figure 7.a*, *Figure 5.b*). Nevertheless sample 3 had approx. the same value for the newly defined separation level and for the 90% level (*Figure 8.b*).

## Conclusions

This study analysed the influence of fabric and yarn construction parameters on the inter-fibre pore structure of plain woven samples by means of a newly developed and Matlab© based image analysis method. The program developed calculated the pore length distribution of inter-fibre pores in the horizontal direction as well as mean pore length values using 2D cross-section images of woven fabrics. Furthermore a scatter diagram with colour bars was constructed to show

how inter-fibre pores are distributed along the yarn cross section. This diagram showed at which level the distribution of pore sizes changes from frequent to rare. A separation level was proposed to distinguish the frequently distributed inter-fibre pores from rarely distributed ones. This separation level was compared with the 90% level. It was proposed that below this level the yarn cross section possesses pores that could be considered as real "inter-fibre pores" as they reflect the real inter-fibre pore characteristics of the cross-section. The results proved that variations in the fabric index affect inter-fibre porosity. Weft yarns with wider lengths and lower heights, which are caused by a decreasing fabric index, tend to have more inter-fibre pores. Distribution results showed that the 90% level of pore lengths changes from 4  $\mu\text{m}$  up to 7.5  $\mu\text{m}$ , which is related to the woven fabric specifications. The difference between the 90% level and separation level was higher for the sample with a smaller fabric index. The sample with a thinner filament fineness showed approximately identical values for the 90% and separation level. This finding proves that in the case of samples of thinner filament fineness, all pore lengths under 90% also exhibit a favorable distribution along the yarn cross-section from top to bottom. In addition, the inter-fibre porosity decreased with a decrease in filament fineness. Weft yarns with textured filaments showed bigger inter-fibre porosity when compared to those with flat filaments. These results could be useful to evaluate the inter-fibre porosities of PES barrier textiles to understand which construction parameters would be more appropriate for the targeted property and to define the separation level between inter-fibre and inter-yarn pore sizes of PES multifilament barrier textiles.

## Acknowledgements

The authors would like to thank to the German Research Foundation (Deutsche Forschungsgemeinschaft) for its support to the research project under project number DFG CH 174/26-2.

## References

1. Rigby AJ, Anand SC, Horrocks AR. Textile materials for medical and healthcare applications. *Journal of the Textile Institute* 1997; 88(3): 83-93.
2. Jain R, Raheel M. Barrier efficacy of woven and nonwoven fabrics used for

- protective clothing: Predictive models. *Bulletin of Environmental Contamination and Toxicology*. 2003; 71(3): 437-446.
3. Nagy V, Vas LM. Pore characteristic determination with mercury porosimetry in polyester staple yarns. *FIBRES & TEXTILES in Eastern Europe* 2005;13, 3(51):21-26.
4. Bénese M, Coq L, Sollic C. Collection efficiency of a woven filter made of multifiber yarn: Experimental characterization during loading and clean filter modeling based on a two-tier single fiber approach. *Journal of Aerosol Science* 2006; 37(8): 974-989.
5. Kuhr M, Aibibu D, Cherif C. Targeted partial finishing of barrier textiles with microparticles and their effects on barrier properties and comfort. *Journal of Industrial Textiles* 2014; 45(5): 853-878.
6. Leonas K, Jinkins R. The relationship of selected fabric characteristics and the barrier effectiveness of surgical gown fabrics. *American Journal of Infection Control* 1997; 25(1): 16-23.
7. Laourine E, Cherif C. Characterization of barrier properties of woven fabrics for surgical protective textiles. *Autex Research Journal*. 2011; 11(2): 31-36.
8. Rief S, Glatt E, Laourine E, Aibibu D, Cherif C, Wiegmann A. Modeling and CFD-Simulation of woven textiles to determine permeability and retention properties. *Autex Research Journal* 2011; 11(3): 78-83.
9. Lankester B, Bartlett G, Garneti N, Blom A, Bowker K, Bannister G. Direct measurement of bacterial penetration through surgical gowns: a new method. *Journal of Hospital Infection* 2002; 50(4): 281-285.
10. Calvin R. Evaluation of the protective value of hospital gowns against blood strike-through and methicillin-resistant staphylococcus aureus penetration. *AORN Journal* 1999; 69(6): 1264-1265.
11. Hellmann A, Rief S, Schmidt K, Kocaman RT, Aibibu D, Cherif C, Ripperger S, Antonyuk S. Simulation der Partikelabscheidung und des Druckverlustes von Schutz- und Filtertextilien bei einer Gasdurchströmung. *Filtrieren & Separieren* 2017; 31(4): 268-274.
12. Burleigh E, Wakeham H, Honold E, Skau E. Pore-Size Distribution in Textiles. *Textile Research Journal* 1949; 19(9): 547-555.
13. Wakeham H, Spicer N. Pore-size distribution in textiles – A study of windproof and water-resistant cotton fabrics. *Textile Research Journal* 1949; 19(11): 703-710.
14. Bhatia SK, Smith JL. Application of the bubble point method to the characterization of the pore-size distribution of geotextiles. *Geotechnical Testing Journal* 1995; 18(1): 94-105.
15. Schwerzt F. The structure of porous materials from gas penetration rates. *Journal of Applied Physics*. 1949; 20(11): 1070-1075.



16. Bhatia S, Smith J. Comparative study of bubble point method and mercury intrusion porosimetry techniques for characterizing the pore-size distribution of geotextiles. *Geotextiles and Geomembranes* 1994; 13(10): 679-702.
17. Li D, Frey MW, Joo YL. Characterization of nanofibrous membranes with capillary flow porometry. *Journal of Membrane Science* 2006; 286(1-2): 104-114.
18. Lee Y, Jeong J, Youn I, Lee, W. Modified liquid displacement method for determination of pore size distribution in porous membranes. *Journal of Membrane Science* 1997; 130(1-2): 149-156.
19. Miller B, Tyomkin I. An Extended Range Liquid Extrusion Method for Determining Pore Size Distributions. *Textile Research Journal* 1986; 56(1): 35-40.
20. Jena A, Gupta K. Liquid extrusion techniques for pore structure evaluation of textile materials. *International Nonwovens Journal* 2003;12: 45-52.
21. Aibibu D, Lehmann B, Offermann P. Barrier effect of woven fabrics used for surgical gowns. *Autex Research Journal* 2003; 3(4): 186-193.
22. Gong RH, Newton A. Image-analysis techniques. Part I: The Measurement of pore-size distribution. *Journal of The Textile Institute* 1992; 83(2): 253-268.
23. She FH, Tung K, Kong L. Calculation of effective pore diameters in porous filtration membranes with image analysis. *Robotics and Computer-Integrated Manufacturing* 2008; 24(3): 427-434.
24. Masselin I, Durand-Bourlier L, Laine J, Sizaret P, Chasseray X, Lemordant D. Membrane characterization using microscopic image analysis. *Journal of Membrane Science* 2001; 186(1): 85-96.
25. Ziel R, Haus A, Tulke A. Quantification of the pore size distribution (porosity profiles) in microfiltration membranes by SEM, TEM and computer image analysis. *Journal of Membrane Science* 2008; 323(2): 241-246.
26. Chang T, Zhang J, Fuch Y. Electrical, mechanical and morphological properties of compressed carbon felt electrodes in vanadium redox flow battery *Journal of Power Sources*. 2014; 245: 66-75.
27. Mühl T, Binnebösel M, Klinge U, Goederz T. New objective measurement to characterize the porosity of textile implants. *Journal of Biomedical Materials Research Part B: Applied Biomaterials* 2007; 84B(1): 176-183.
28. Klinge U, Otto J, Mühl T. High structural stability of textile implants prevents pore collapse and preserves effective porosity at strain. *BioMed Research International* 2015; 2015:1-7.
29. Walz F, Luibrand J. Die Gewebedichte. *Textil Praxis Bd* 1947; 2: 330-335.

☐ Received 22.03.2018 Reviewed 10.05.2018



## INSTITUTE OF BIOPOLYMERS AND CHEMICAL FIBRES

### IBWCh LABORATORY OF BIODEGRADATION

The Laboratory of Biodegradation operates within the structure of the Institute of Biopolymers and Chemical Fibres. It is a modern laboratory with a certificate of accreditation according to Standard PN-EN/ISO/IEC-17025:2005 (a quality system) bestowed by the Polish Accreditation Centre (PCA). The laboratory works at a global level and can cooperate with many institutions that produce, process and investigate polymeric materials. Thanks to its modern equipment, the Laboratory of Biodegradation can maintain cooperation with Polish and foreign research centers as well as manufacturers and be helpful in assessing the biodegradability of polymeric materials and textiles.

The Laboratory of Biodegradation assesses the susceptibility of polymeric and textile materials to biological degradation caused by microorganisms occurring in the natural environment (soil, compost and water medium). The testing of biodegradation is carried out in oxygen using innovative methods like respirometric testing with the continuous reading of the CO<sub>2</sub> delivered. The laboratory's modern MICRO-OXYMAX RESPIROMETER is used for carrying out tests in accordance with International Standards.



The methodology of biodegradability testing has been prepared on the basis of the following standards:

- **testing in aqueous medium:** 'Determination of the ultimate aerobic biodegradability of plastic materials and textiles in an aqueous medium. A method of analysing the carbon dioxide evolved' (PN-EN ISO 14 852: 2007, and PN-EN ISO 8192: 2007)
- **testing in compost medium:** 'Determination of the degree of disintegration of plastic materials and textiles under simulated composting conditions in a laboratory-scale test. A method of determining the weight loss' (PN-EN ISO 20 200: 2007, PN-EN ISO 14 045: 2005, and PN-EN ISO 14 806: 2010)
- **testing in soil medium:** 'Determination of the degree of disintegration of plastic materials and textiles under simulated soil conditions in a laboratory-scale test. A method of determining the weight loss' (PN-EN ISO 11 266: 1997, PN-EN ISO 11 721-1: 2002, and PN-EN ISO 11 721-2: 2002).



AB 388



The following methods are applied in the assessment of biodegradation: gel chromatography (GPC), infrared spectroscopy (IR), thermogravimetric analysis (TGA) and scanning electron microscopy (SEM).

#### Contact:

INSTITUTE OF BIOPOLYMERS AND CHEMICAL FIBRES  
ul. M. Skłodowskiej-Curie 19/27, 90-570 Łódź, Poland  
Katarzyna Dziedziczak Ph. D.,  
tel. (+48 42) 638 03 31, e-mail: lab@ibwch.lodz.pl